Numerical modelling of the 1970 intraslab Peru earthquake and tsunami (Mw 7.9)

César Jiménez · Miguel Saavedra J. ·
Yolanda Zamudio · Daniel Olcese

Abstract In this research paper, we have modelled
the tsunami source of the 1970 Peruvian earthquake.
The rupture geometry (of dimensions 150×75 km^2)
was obtained from the aftershocks distribution. The
fault plane geometry was divided into 2 subfaults: the
biggest (of 112.5-km length to the northern side) of
normal fault plane and the smallest (37.5-km length
to the south) of reverse fault plane, due to the seis-
mic event had a complex rupture process. The slip
was constrained from the tsunami waveform ampli-
tudes and seismic moment using an iterative approach
method, since a data inversion is impossible due to
the scarcity of available tsunami data. The simulated
vertical deformation field has a particular pattern, it
is composed of 4 lobes of alternated uplift and subsi-
dence, the maximum subsidence was 38 cm, and the
maximum uplift was 57 cm. We have obtained a seis-
mic moment of 8.92×10^{20} Nm and the corresponding
moment magnitude was Mw 7.9. The maximum slip
was calculated in 1.59 m (reverse fault) and 1.32
m (normal fault). The simulated maximum tsunami
height was 93 cm at Salaverry and 73 cm at Chimbote
stations.

C. Jiménez (✉) · M. Saavedra J. · Y. Zamudio
Universidad Nacional Mayor de San Marcos, Lima, Peru
e-mail: cjimenezt@unmsm.edu.pe

D. Olcese
Universidad Nacional de Ingeniería, Lima, Peru

1 Introduction

The teleseismic waveforms of old long period stations
have been used by Abe (1972) and Beck and Ruff
(1989) to constrain the focal mechanism of the Mw7.9
Peru (May 31, 1970) and other earthquakes; how-
ever, there is not research on the slip distribution for
this unusual event (seismic source with normal fault
and reverse fault). Unfortunately, the tsunami record-
ings from the Chimbote and Callao stations were lost
and there is not any geodetic data on that date. How-
ever, it is possible to investigate and constrain the
slip amplitude of this event based on seismic data
(aftershocks distribution and focal mechanism), his-
torical information of macroseismic intensities, and
maximum tsunami data reported on the literature.
Similar research has been conducted by Jiménez and
Moggiano (2020) for the 1940 Peruvian earthquake.

The idealized inversion technique would be a
joint inversion of teleseismic together with geodetic
and tsunami data. Slip models derived from various
datasets are more reliable than those that consider a
single set of data because they should be more con-
strained (Ioualalen et al. 2013). Unfortunately, this is
not the case for the 1970 Peru earthquake.

Most tsunamis are generated by thrust earthquakes
located offshore. However, some normal fault plane

earthquakes have generated tsunamis. For example, the large 1933 Sanriku earthquake generated a big tsunami (Kanamori 1971), while the intraslab 2017 Mexico earthquake of magnitude Mw 8.2 (Jiménez 2018) and the 1970 Peruvian earthquake (Mw 7.9) generated small tsunamis (maximum amplitude less than 1 m).

One of the most catastrophic events in the history of Peru occurred on May 31, 1970, as an earthquake shook Peru and took almost 70,000 lives (most due to the cataclysmic debris in the cities Yungay and Ranrahirca in Ancash). The earthquake caused 50,000 injuries and destroyed or rendered uninhabitable roughly 186,000 buildings (Ericksen et al. 1970).

The shaking of the 1970 Peruvian earthquake was strongly felt near the seismic source: Chimbote, Casma, and Huarmey (intensity VIII MM), in Lima was felt with intensity VI; in Nazca and Ica was felt with an intensity of II. To the north, the earthquake was felt as far as Guayaquil Ecuador (intensity II).

The tsunami generated by the 1970 Peruvian earthquake was small (with amplitude less than 1 m), recorded only in tidal gauges of Chimbote and Callao, in the near field; unfortunately, these tsunami recordings are lost. There is not reports about destruction due to the tsunami inundation; however, in Chimbote, the runup was around 2 m, without any damages. No tsunami was observed at the stations of Talara, San Juan de Marcona, and Matarani (Lomnitz 1970). However, the tsunami reached the Japanese coast (https://www.ngdc.noaa.gov/hazel/view/hazards/tsunami/runup-data?sourceMaxYear=1970&sourceMinYear=1970&sourceCountry=PERU).

In this research, we have estimated the tsunami source of the 31 May 1970 (Mw 7.9) Peru earthquake from seismic data and sparse tsunami data. This is also known as the great Peruvian earthquake because of the large destruction and a high number of casualties it caused (70 thousand). Given the scarcity of available tsunami data, since a data inversion is impossible, we have attempted to constrain the coseismic slip using an iterative approach that minimizes the comparison between the following: (i) two observed and synthetic peak-to-trough tsunami amplitudes and (ii) the earthquake seismic moment estimated by Beck and Ruff (1989). Any attempt to unveil the characteristics of a seismic source is a worthwhile one, and particularly in this case, because the earthquake is also known from

the literature to have been generated by a complex source.

1.1 Background of previous research

Some researchers have investigated the seismological aspects of the 1970 Peruvian earthquake, for example:

Lomnitz (1971) conducted a preliminary analysis on the 1970 Peruvian earthquake, and he stated that this event was a multiple shock event, consisting of several close shocks at different depths and perhaps with different focal mechanism; however, he did not calculate the focal mechanism.

Cluff (1971) conducted a field survey for the geology aspects of the 1970 Peru earthquake. He described the seismic activity of the earthquake, as well as its characteristics and effects on: active fault lines and debris avalanches in the cities of Yungay and Ranrahirca (close to Huascarán mountain), and damage in the coastal region.

Abe (1972) conducted the calculation of the focal mechanism of the 1970 Peru earthquake from teleseismic surface waves. He obtained a normal fault plane (strike=340°, dip=53°, rake=−90°) and a moment magnitude of Mw 7.9. He concluded that the rupture was inside the subducting Nazca plate. He did not take into account the complexity of the seismic source.

Stauder (1975) calculated the focal mechanism of the mainshock (normal fault type) and of 3 aftershocks located to the southeast from the epicenter; these were thrusted faults. He concluded that either the fracture occurred within the plate and is related to the flexure as the plate begins to descend, or to the axial tension under gravitational stress.

Dewey and Spence (1979) have recalculated the aftershocks hypocenters (for 1970 earthquake) using the method of joint hypocenter determination (JHD). They have identified two cluster groups of aftershocks: one of them around the epicenter in the northern side (where the normal faulting mainshock occurred) and the other one in the southern side.

Beck and Ruff (1989) used the teleseismic P-waveforms inversion to constrain the focal mechanism and the source time function. They assumed that "the aftershock complexity reflects the mainshock complexity. Therefore, the mainshock was a double event with two different focal mechanisms and depths.". These two subevents had a time delay, first occurred

the normal fault plane subevent and 40 s after, the inverse fault plane subevent. They obtained the seismic moment from undiffracted P-waves as 1.6×10^{21} Nm and the corresponding moment magnitude was Mw 8.0.

By means of an iterative approach, we modelled the tsunami source of the 1970 Peru dual focal mechanism earthquake using tsunami numerical modelling. We have estimated the slip amplitude, the scalar tsunami moment, and tsunami waveforms at 5 tidal stations in the near field.

1.2 Seismotectonic setting and historical seismicity

The occurrence of major earthquakes (Mw>7.0) in Peru is a corollary of the subduction of the Nazca Plate under the South American Plate, with a convergence speed of 6–7 cm/year (Norabuena et al. 1998). The

rupture geometry of the 1970 Peruvian earthquake is located in the boundary of the northern and central region of Peru (Fig. 1). The northern region of Peru is limited by the Mendaña Fracture Zone to the south and the Alvarado Ridge to the north. On the other hand, the central region of Peru is limited by two tectonic elements: the Mendaña Fracture Zone to the north and the Nazca Ridge to the south, separated by a distance of 600 km. These tectonic elements act as a barrier for the seismic rupture propagation (Jiménez et al. 2021).

According to Barazangi and Isacks (1976), "the seismic profile in the north and central region of Peru indicates a flat or normal subduction, with absence of Quaternary volcanic activity."

The Mendaña Fracture Zone divides the Nazca plate in two tectonic environments that behave differently. The central region of Peru is characterized by high interseismic coupling, while the northern region

Fig. 1 Seismotectonic setting of the northern and central Peru region. The black rectangle represents the 1970 rupture geometry. The pink ellipses represent the fault geometry of 1619, 1725 and 1746 Callao earthquake (~Mw9.0). The focal diagrams represent the locations of events of the seismic sequence of 20th and 21st centuries
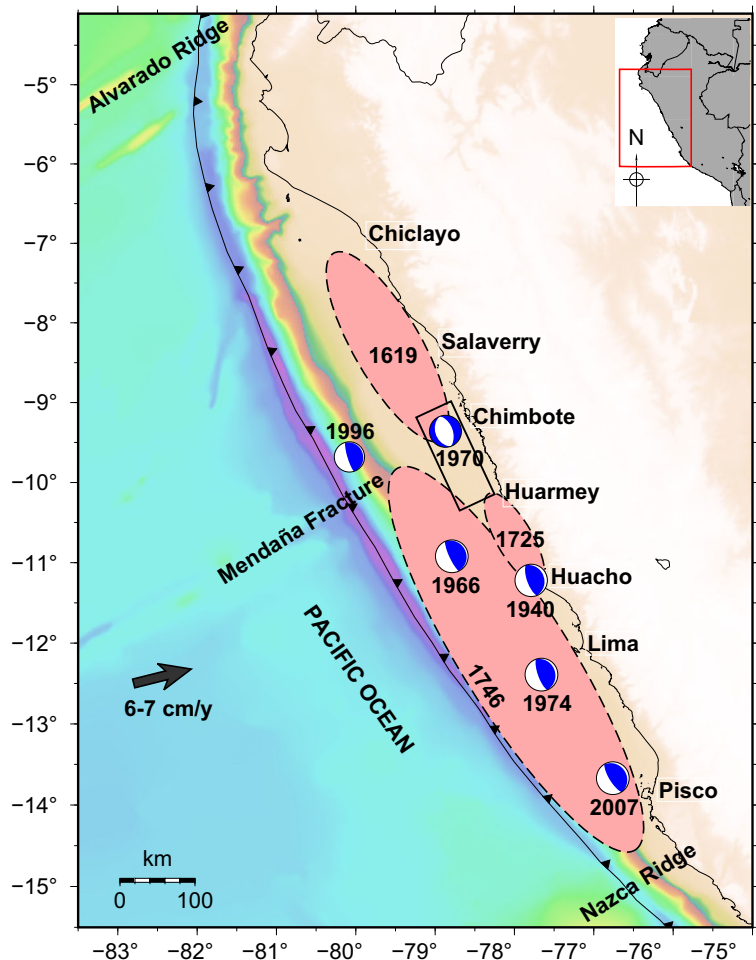
of Peru is characterized by low interseismic coupling (Villegas et al. 2016). The 1970 seismic source geometry is located on the extension of the Mendaña Fracture Zone, where the interseismic coupling is very low (Fig. 1).

The rupture geometry of the 1970 earthquake is located to the north of the 1725 earthquake and 1940 thrust earthquake (Jiménez and Moggiano 2020), to the south and partially overlapping with the 1619 earthquake and to the east of the northern side of the rupture geometry of the 1966 thrust earthquake (Jiménez et al. 2022). The 1996 tsunami earthquake is located offshore Chimbote and close to the Peruvian trench (Fig. 1).

The catalogues of historical seismicity (from the arrival of the spanish conquerors in 1500 AD) include the occurrence of two large events in the northern region of Peru: 1619 and 1725 (Silgado 1978). A large event was also recorded in the central region of Peru in 1746, whose rupture area covers from Pisco to Chimbote (Jiménez et al. 2013; Mas et al. 2014).

On February 14, 1619, an earthquake occurred in the northern region of Perú. The isoline of VIII intensity for the 1619 event affected everything between the city of Casma (the the south) to Chiclayo (in the north). The earthquake killed 350 people and left an estimated 130 victims buried in the rubble. In Trujillo, the buildings and temples collapsed. The destruction spread to the valleys of Santa (Chimbote) and Saña (Lambayeque) (Silgado 1978; Dorbath et al. 1990).

On January 6, 1725, a strong earthquake caused severe damages in Trujillo. In the snowy mountains of the Cordillera Blanca, a glacial lagoon collapsed and overflowed, killing 1500 people and devastating the city of Yungay. The earthquake was felt in Lima (Silgado 1978). The most important damage was reported along the coast, between latitudes from $-10°$ to $-11°$ and the intensity could have reached VIII. It is possible that this event could be an intraplate event inside the subducting Nazca Plate, similar to the 1970 earthquake (Dorbath et al. 1990).

2 Data

The information of the historical reports and macroseismic effects have been taken from Dorbath et al. (1990) and Silgado (1978). The seismic and hypocentral parameters (Table 1) have been taken from Beck

Table 1 The parameters of the hypocenter of the 1970 Peru earthquake were reported by Beck and Ruff (1989). Abe (1972) calculated the focal mechanism

Date	May 31, 1970
Origin time	20:23 UTC
Latitude	$-09.36°$
Longitude	$-78.87°$
Depth	50 km
Magnitude	7.9 Mw
Strike	$\theta = 340°$
Dip	$\delta = 53°$
Rake	$\lambda = -90°$

and Ruff (1989). Abe (1972) calculated the focal mechanism parameters, in particular the strike angle was 340°; based on the most updated subduction model (Hayes et al. 2018), the average slab strike in the source location is 330°; therefore, we have slightly modified the strike angle to a mean value of 335°, in this way the fault plane geometry orientation would be aligned with the trench and coastline orientation (Fig. 2). However, we have conducted a sensitivity test of the strike angle to fit the data (Fig. 4).

The aftershocks distribution for a time window of one month (small circles in red color in Fig. 2) has been taken from the USGS catalogue (https://earthquake.usgs.gov/earthquakes/map/). According to Lomnitz (1971), most of the aftershocks are consistent with the mainshock in their directions of the first motion; however, there are some aftershocks with their polarity inverted.

Intensity information must be carefully interpreted when it is used to determine earthquake rupture geometry (Kelleher 1972). The high macroseismic intensities (VIII MM in Fig. 2) reported in the Callejón de Huaylas must be connected with the local geology that generated the avalanche rather than to the shaking due to the earthquake. However, the extremes of the fault plane (in Fig. 2) fit well with the isoline of intensity VIII.

The tsunami recordings for the 1970 event are lost. However, according to Lomnitz (1970), 12 min after the start of the earthquake, the tide gauge at Chimbote recorded a disturbance (possibly due to swell), followed by a tsunami waveform. The initial downward motion of the sea level was of the order of 1 ft (1 ft = 30.48 cm) and the total peak-to-trough amplitude
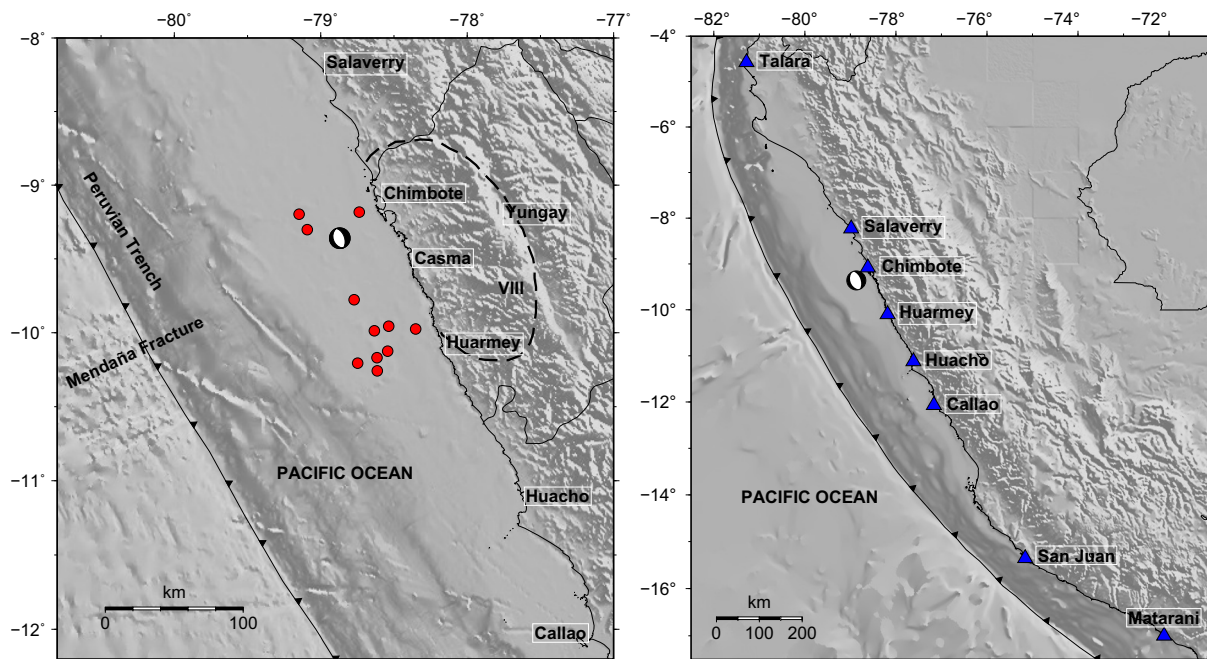
Fig. 2 a The aftershock distribution of the 1970 Peru earthquake from USGS (small red circles) and VIII isoseismal intensity (dashed line) from Silgado (1978). b The blue triangles represent the tidal gauges used in this research. The focal diagram is located at the epicenter

of the tsunami did not exceeded 3 ft. The tsunami was also recorded on the tide gauge at Callao, with a total amplitude of around 1 ft, the arrival time was between 1 and 1.5 h after the earthquake, but the beginning was obscured by noise. No tsunami was observed at the stations at Talara, San Juan de Marcona, and Matarani. Also, no evidence of coastal uplift or subsidence has been reported. We recognize that the tsunami data is

very poor to constrain the model; however, we do not have additional data (Table 2).

The bathymetry data was obtained from the Gebco 15 model (www.gebco.net), with a resolution of 15 arcsecond or approximately 466 m. This global bathymetry has been combined with finer bathymetry from the Peruvian Navy and finer topography from satellite images (SRTM1: http://www2.jpl.nasa.gov/

Table 2 Tidal stations and simulated tsunami parameters. N represents the number of the tidal station. H_{max} is the maximum tsunami height and Ta is the tsunami arrival time of the first wave, either positive or negative

N	Station	Lat (°)	Lon (°)	H_{max} (m)	Ta (min)
1	Talara	−04.5751	−81.2827	0.02	45
2	Salaverry	−08.2279	−78.9818	0.93	23
3	Chimbote	−09.0800	−78.6170	0.73	32
4	Huarmey	−10.0992	−78.1824	0.24	05
5	Huacho	−11.1218	−77.6162	0.47	50
6	Callao	−12.0689	−77.1668	0.27	62
7	Marcona	−15.3556	−75.1603	0.03	64
8	Matarani	−17.0010	−72.1088	0.01	96

srtm) at Salaverry, Chimbote, Huarmey, Huacho, and Callao, where the tsunami waveforms were calculated. The data was interpolated using the Kriging method to obtain a digital elevation model with a resolution of 10 arcsecond (approximately 309 m).

3 Methodology

3.1 Fault plane scenario

The aftershock distribution constrains the dimensions of the fault plane geometry, with a length $L = 150$ km and a width $W = 75$ km (Fig. 2). This fault plane geometry is located offshore and very close to the coastline; its extremes (in the strike direction) are located according to the isoline of macroseismic intensity VIII.

According to Beck and Ruff (1989), the first pulse of moment release occurred between the epicenter and 75 km to the southeast within the second cluster of aftershocks. This result indicates that the mainshock rupture overlaps with the cluster of aftershocks with a down dip compression. Furthermore, according to Beck and Ruff (1989) "the second source is about one-third to one-quarter the size of the first source." Therefore, we have divided the fault plane into two subfaults, the biggest ($3L/4$=112.5-km length) of normal focal mechanism and the smallest ($L/4$=37.5-km length) of reverse focal mechanism, according to Table 3.

The upperside depth of the subfaults were constrained geometrically, according to location of the

Table 3 The fault plane parameters of the 1970 Peru earthquake. (X_0, Y_0) is the position of the lowerside corner of the source geometry. Z_0 is the upperside depth of the subfault

Parameter	Fault 1	Fault 2
X_0	−78.7553°	−78.6841°
Y_0	−09.9751°	−10.3068°
Z_0 (km)	40	10
L (km)	112.5	37.5
W (km)	75.0	75.0
Slip (m)	1.32	1.59
Strike	348°	348°
Dip	53°	50°
Rake	−90°	90°

hypocenter and to focal mechanism parameters. The upperside depth Z_0 of the subfault 1 was fixed at 40 km, taking into account a focal depth of 50 km, while the upperside depth of the subfault 2 was fixed at 10 km for a focal depth of 30 km (Table 1), according to the constrains of Beck and Ruff (1989).

All the seismic source parameters (focal mechanism, subfault dimensions, subfault location) are fixed, except the slip. To obtain the slip, we have used an iterative approach method with the tsunami numerical modelling. The constraints are the amplitudes of the first period or cycle of the tsunami waveform at Chimbote and Callao tidal stations, reported by Lomnitz (1970), and the seismic moment obtained by Beck and Ruff (1989).

3.2 Tsunami numerical modelling

In this investigation, we have used the linear shallow water equations to simulate the tsunami propagation along the Pacific Ocean. As was demonstrated by Jiménez and Moggiano (2020), the first tsunami waveform period of the linear model correlates very well with that of the corresponding non-linear model. However, we have used a non-linear model to simulate the tsunami propagation around Chimbote and Callao stations.

To obtain the initial condition for tsunami propagation, we have calculated the vertical coseismic deformation pattern, using the formulation of Mansinha and Smylie (1971) and the seismic source parameters from Table 3, considering an elastic, homogeneous, linear, and semi-infinite medium. As an approximation, we consider that the sea surface deformation is equal to that of the sea bottom deformation.

We have taken into account the time delay of 40 s between the two subevents, in the tsunami numerical modelling. In the first seconds, the numerical model takes into account the deformation due to the normal fault plane subevent (Fault 1) and 40 s after the deformation due to the inverse fault plane subevent (Fault 2) (Table 3).

In the general case, the governing non-linear differential equations in cartesian coordinates are expressed as:

$$\frac{\partial \eta}{\partial t} + \frac{\partial M}{\partial x} + \frac{\partial N}{\partial y} = 0 \tag{1}$$

$$\frac{\partial M}{\partial t} + \frac{\partial}{\partial x}\left(\frac{M^2}{D}\right) + \frac{\partial}{\partial x}\left(\frac{MN}{D}\right) = -gD\frac{\partial \eta}{\partial x}$$
$$-\frac{gn^2}{D^{7/3}}M\sqrt{M^2 + N^2} \qquad (2)$$

$$\frac{\partial N}{\partial t} + \frac{\partial}{\partial x}\left(\frac{MN}{D}\right) + \frac{\partial}{\partial x}\left(\frac{N^2}{D}\right) = -gD\frac{\partial \eta}{\partial x}$$
$$-\frac{gn^2}{D^{7/3}}N\sqrt{M^2 + N^2} \qquad (3)$$

where M and N represent the flow discharge for the direction x and y respectively, η is the water level, and h is the depth of the water with respect to mean sea level and $D = \eta + h$.

We have used the non-linear TUNAMI numerical model (Imamura et al. 2006) to simulate the tsunami propagation and inundation in Chimbote and Callao. We have used a fine bathymetry with a grid size of 1 arcsecond (~31 m) in four nested grids.

In the rest of the stations, the tsunami propagation process has been simulated using the linear TUNAMI numerical model. We have used a bathymetry with a grid size of 10 arcsecond (~309 m). We have located the tide gauge stations in coastal cities (most of them correspond to real tide gauges, except the virtual tide gauge of Huarmey) to obtain simulated tsunami waveforms (Table 2). The computational grid, to perform the linear tsunami simulation, has a dimension of 2521×2566 columns and rows respectively. The geographical limits are as follows: $-7.0°$ to the north, $-14.0°$ to the south, $-83.0°$ to the west, and $-76.0°$ to the east.

To obtain the tsunami waveforms for Talara, Marcona, and Matarani stations, we have conducted a linear tsunami simulation with a computational grid size of 15 arcsecond, and the geographical limits are as follows: $-3.0°$ to the north, $-18.0°$ to the south, $-84.0°$ to the west, and $-70.0°$ to the east.

3.3 Iterative approach method

Because it is not possible to use an inversion method (because of the lack of tsunami waveforms), we have used an iterative approach method to constrain the slip. This is a forward method which consists of numerical simulation and compared to the results of the available information.

The tsunami waveforms in each station are expressed as a linear combination of the simulated waveforms or Green's functions:

$$d_i(t) = \sum_{j=1}^{2} m_j G_{ij}(t) \qquad (4)$$

where $G_{ij}(t)$ is the time-dependent Green's function in the ith tidal station generated by the jth subfault, m_j is the value of the slip in the jth subfault, and $d_i(t)$ is the simulated tsunami waveform in the ith station (Jiménez et al. 2018).

To constrain the slip (m_1 and m_2 in (4)), we have used the report of Lomnitz (1970): the total peak-to-trough amplitude of the tsunami (at Chimbote station) was around 3 ft. The total amplitude of the tsunami on the tide gauge at Callao was around 1 ft (1 ft=30.48 cm). In the case of the Chimbote station, the peak-to-trough amplitude is obtained within the first period or cycle of the tsunami waveform.

We have used the iterative approximation method, in which some parameters are fixed and the rest are varied until a minimum normalized variance is obtained between the observed and simulated data. In this case, we have varied the slip: $1.26 < m_1 < 1.38$ m and $1.48 < m_2 < 1.70$ m. A metric to evaluate the correlation would be the normalized variance, which is defined as:

$$\text{var} = \frac{\sum_{k=1}^{N_k}[\text{obs}(k) - \text{sim}(k)]^2}{\sum_{k=1}^{N_k}[\text{obs}(k)]^2} \qquad (5)$$

where $\text{obs}(k)$ represents the observed variable, $\text{sim}(k)$ is the simulated variable, and $N_k = 3$ is the number of data (tsunami amplitude at Chimbote and Callao stations and seismic moment). Figure 3 shows the sensitivity test to find the parameters m_1 and m_2. After several attemps, and based on Lomnitz (1970) tsunami report on amplitudes at Chimbote and Callao stations and seismic moment reported by Abe (1972), we have obtained a slip value of m_1=1.32 m (normal fault) and m_2=1.59 m (reverse fault). The minimum normalized variance was var = 4.43×10^{-7} (Fig. 3).

3.4 Sensitivity test for strike angle estimation

We have conducted a sensitivity test to constrain the strike angle. We have fixed the slip of the two subfaults ($m_1 = 1.32$ m and $m_2 = 1.59$ m) and we have varied the strike angle from 331 to 356°. The seismic moment M_o was weighted by a factor of 10^{-21}. The

Fig. 3 Sensitivity test to calculate slip 1 (1.32 m) and slip 2 (1.59 m). The vertical lines indicate the position of the minimum value of normalized variance (var = 4.43×10^{-7})
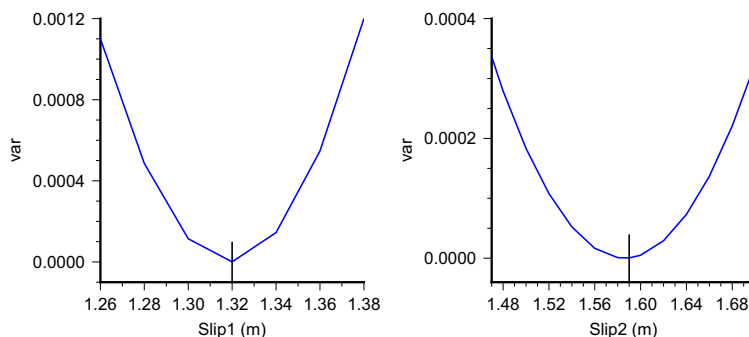
minimal normalized variance was obtained using the (5) and corresponds to the strike = 348° (Fig. 4).

The effect of strike angle value estimated (348°), is to bring near the northern side of the fault to the continent, as we can show in Fig. 5a.

4 Results and discussion

The tsunami source estimated in this research is consistent with the kinematic source discussed in Beck and Ruff (1989).

4.1 Seismic source

According to Table 3, the fault plane geometry has been divided in two subfaults: the northern subfault of normal focal mechanism with slip 1.32 m and the southern subfault of reverse focal mechanism with slip 1.59 m. These slips were constrained with the amplitudes of tsunami waveforms of Chimbote and Callao
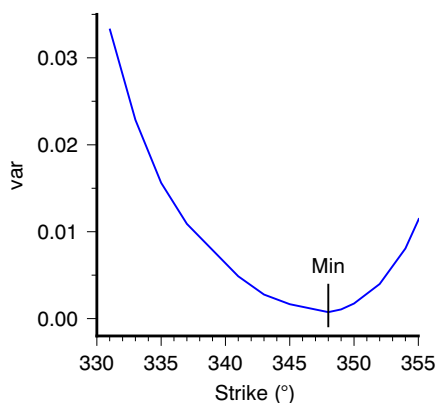

Fig. 4 Sensitivity test to calculate the strike angle. The minimal normalized variance (var) corresponds to strike angle of 348°

stations. The subfault with normal focal mechanism overlaps the cluster aftershock region of reverse focal mechanism, according to Beck and Ruff (1989).

The estimated slip is different for each subfault. We do not have additional information (as tsunami waveforms) to constrain the slip distribution using an inversion method.

According to mean rigidity constant of Table 4, we have calculated a total tsunami moment of 8.92×10^{20} Nm and the corresponding moment magnitude was Mw 7.9. The proportion of seismic moment is $M_1 / M_2 \approx 3$. This result is similar to that obtained by Abe (1972), based on seismic surface waves. However, Beck and Ruff (1989) calculated a moment magnitude of Mw 8.0, based on undiffracted P-waves.

4.2 Coseismic deformation field

The simulated vertical deformation field has a particular pattern, composed of 4 lobes of alternated uplift and subsidence (Fig. 5). The effect of the high dip normal faulting (coastal subsidence in the northern side) prevails over the pattern of the high dip reverse faulting (coastal uplift in the southern side).

According to these results, the city of Chimbote subsided around 12 cm and the city of Huarmey was uplifted around 2.5 cm. The maximum simulated subsidence was 38 cm and the maximum uplift was 57 cm. Unfortunately, there was not geodetic data in 1970 to compare these results.

4.3 Tsunami simulation

We have obtained the simulated tsunami waveforms from 5 tidal stations in the near field (Table 2). The maximum wave height was 0.93 m at Salaverry and 0.73 m at Chimbote stations. In Chimbote, the sea
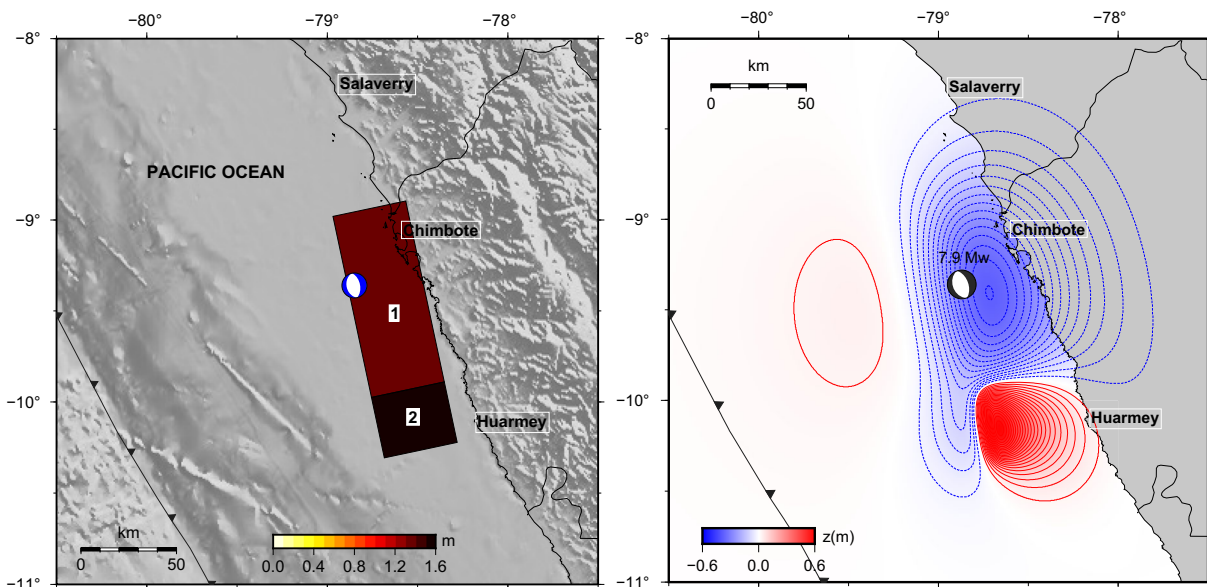
Fig. 5 a Slip distribution of the 1970 Ancash earthquake. b Simulated vertical deformation field. The blue zone represents the subsidence region and the red represents the uplifted region.

The focal mechanism diagram is located on the epicenter. The isolines represents 2.5 cm

receded and after 32 min, the first tsunami waveform arrived, due to this station is located within the seismic source geometry.

The simulated maximum tsunami wave height at Callao station was 0.27 m (according to Lomnitz (1970) report of 1 ft) and the arrival time was 62 min (Fig. 6).

There is not an important effect of taking into account the time delay between the two subfaults, as we can noticed on Fig. 6. The tsunami waveforms in red color correspond to an instantaneous coseismic deformation and they are superimposed to that of delayed seismic source (in blue color). According to Abe (1972), the seismic rupture velocity was 2.5 km/s much greater than the mean tsunami velocity of 0.2 km/s; therefore, the effects of the time delay of the seismic source on tsunami propagation are negligible.

From Fig. 6, we noticed that the polarity waveforms of Salaverry and Chimbote stations are negatives according to the sudsidence pattern in the northern side of the rupture geometry, while the polarity waveforms of Huarmey, Huacho, and Callao stations are positives according to coseismic uplift pattern.

According to Lomnitz (1970), no tsunami was observed at the stations of Talara, San Juan de Marcona, and Matarani. These observations corroborated the results of the numerical simulation for these stations, where the maximum amplitudes were 2, 3, and 1 cm at Talara, Marcona, and Matarani, respectively (Fig. 7). These amplitudes were not observable due to these were of the same level than the sea level noise.

4.4 Tectonic implications

The location of the rupture geometry of the 1970 earthquake occurs where the Mendaña Fracture Zone enters the trench (Fig. 2). This tectonic element can affect the complexity of the seismic source of this dual focal mechanism event. The Mendaña Fracture Zone
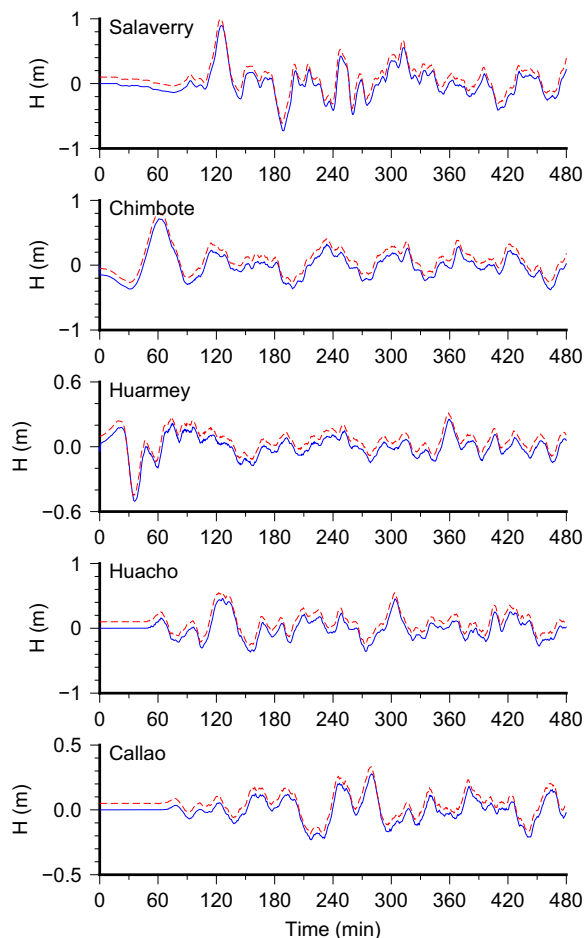
Table 4 The elastic coefficient (μ) and seismic moment (M_o) parameters for each subfault of the 1970 Peru earthquake

Parameter	Fault 1	Fault 2
μ (N/m^2)	6.0×10^{10}	5.0×10^{10}
M_o (Nm)	6.68×10^{20}	2.24×10^{20}
M_w	7.8	7.5

Fig. 6 Simulated tsunami waveforms. In blue color: from delayed seismic source. In red color: from not-delayed seismic source. Notice that they are almost superimposed

Fig. 7 Simulated tsunami waveforms for Talara, Marcona, and Matarani stations. Notice that the maximum amplitude is not greater than 4 cm

5 Conclusions

We have modeled the tsunami source of an unusual earthquake of dual focal mechanism: 75% of normal fault plane and 25% of reverse fault plane. The nature of this seismic source is related with the presence of the Mendaña Fracture Zone, which divides the Nazca plate in two tectonic environments with different behavior.

Despite the fact that there was a time delay of 40 s in the seismic rupture process, the effects of the time delay of the seismic source on tsunami propagation were negligible in this case, due to the seismic rupture velocity of 2.5 km/s was much greater than the mean tsunami velocity of 0.2 km/s.

We have constrained the slips to 1.32 m and 1.59 m for normal fault and reverse fault respectively. However, it is not possible to constrain the slip distribution (for several subfaults) because we do not have enough information and data (for example, tsunami waveforms).

The vertical coseismic deformation field has a particular pattern (because of the dual focal mechanism of the event), with 4 lobes of alternated zones of uplift and subsidence. The simulated maximum uplift was 57 cm and the maximum subsidence was 38 cm.

and the 1970 Peruvian earthquake form the boundary between two subduction zones with very different behavior (Beck and Ruff 1989).

According to the results of Beck and Ruff (1989), the seismic rupture is of dual nature with two focal mechanism, the region around the epicenter had a normal fault mechanism and the southern region had a reverse focal mechanism. This is in accordance to the coseismic deformation pattern in Fig. 5.

The map of interseismic coupling (Fig. 8) obtained by Villegas et al. (2016) shows relevant asperity in the Peruvian central zone. After the occurrence of the 1970 Peruvian earthquake (close the coastline) and the 1966 earthquake (between the trench and the coast), there is not asperities in the 1970 rupture geometry.
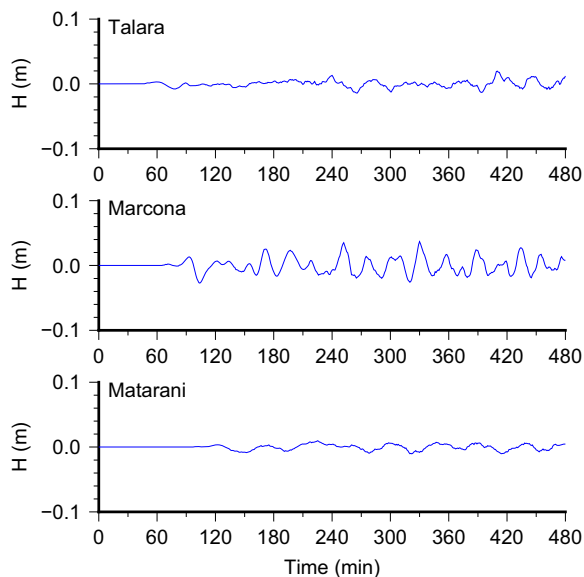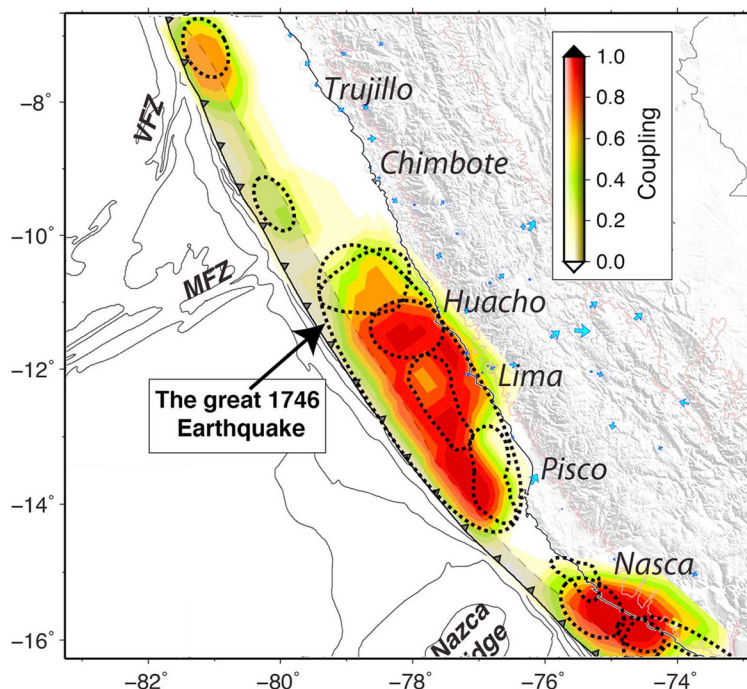
Fig. 8 Average interseismic coupling model of Peru, superimposed with large earthquake ruptures. Modified from Villegas et al. (2016)

Having constrained the slip, we calculated the scalar tsunami moment as 8.33×10^{20} Nm and the corresponding moment magnitude was Mw 7.9. This is similar to the magnitude calculated by Abe (1972), from teleseismic surface waves.

The polarity of the tsunami waveforms is according to location of the lobes of uplift and subsidence. The tsunami waveforms of Salaverry and Chimbote have negative polarity, while the tsunami waveforms of Huarmey, Huacho, and Callao have positive polarity. The maximum tsunami wave height (0.93 m) was calculated at Salaverry station.

The 1970 Peruvian tsunami was only detected by the tidal stations in the near field. This tsunami does not caused any damage on the infrastructure and facilities at ports and beach resorts in the Peruvian coast.

Compliance with Ethical Standards

Conflict of interest   Not applicable.

References

Abe K (1972) Mechanism and tectonic implications of the 1966 and 1970 Peru earthquakes. Phys Earth Planet Inter 5:367–379

Barazangi M, Isacks B (1976) Spatial distribution of earthquakes and subduction of the Nazca plate beneath South America. Geol 4:686–692

Beck S, Ruff L (1989) Great earthquakes and subduction along the Peru trench. Phys Earth Planet Inter 57:199–224

Cluff L (1971) Peru earthquake of may 31, 1970: engineering geology observations. Bull Seismol Soc Am 61(3):511–533

Dewey J, Spence W (1979) Seismic gaps and zones of recent large earthquakes in coastal Peru. Pure Appl Geophys 117:1148–1171

Dorbath L, Cisternas A, Dorbath C (1990) Assessment of the size of large and great historical earthquakes in Peru. Bull Seismol Soc Am 80(3):515–576

Ericksen G, Plafker G, Fernandez J (1970) Preliminary report on the geologic events associated with the may 31, 1970, Peru earthquake. Technical Report 639, USGS

Hayes G, Moore G, Portner D, Hearne M, Flamme H, Furtney M, Smoczyk G (2018) Slab2, a comprehensive subduction zone geometry model. Science 362(6410):58–61

Imamura F, Yalciner A, Ozyurt G (2006) Tsunami modelling manual (TUNAMI model). Tohoku University, Sendai, 1st edn

Ioualalen M, Perfettini H, Yauri S, Jiménez C (2013) Tsunami modeling to validate slip models of the 2007 Mw8.0 Pisco earthquake, central Peru. Pure Appl Geophys 170:433–451

Jiménez C (2018) Seismic source characteristics of the intraslab 2017 chiapas-Mexico earthquake (Mw8.2). Phys Earth Planet Inter 280:69–75

Jiménez C, Carbonel C, Rojas J (2018) Numerical procedure to forecast the tsunami parameters from a database of pre-simulated seismic unit sources. Pure Appl Geophys 175:1473–1483

Jiménez C, Carbonel C, Villegas-Lanza J, Quiroz M, Wang Y (2022) Seismic source of 1966 Huacho Peru earthquake (Mw 8.1) from tsunami waveform inversion. Pure Appl Geophys 179

Jiménez C, Luna N, Moreno N, Saavedra M (2021) Seismic source characteristics of the intermediate-depth and intraslab 2019 northern Peru earthquake (Mw 8.0). J Seismol 25:863–874

Jiménez C, Moggiano N (2020) Numerical simulation of the 1940 lima-Peru earthquake and tsunami (Mw 8.0). J Seismol 24(1):89–99

Jiménez C, Moggiano N, Mas E, Adriano B, Koshimura S, Fujii Y, Yanagisawa H (2013) Seismic source of 1746 Callao earthquake from tsunami numerical modelling. J Disaster Res 8(2):266–273

Kanamori H (1971) Seismological evidence for a lithospheric normal faulting - the Sanriku earthquake of 1933. Physi Earth Planet Interiors 4:289–300

Kelleher J (1972) Rupture zones of large south american earthquakes and some predictions. J Geophys Res 27:2087–2103

Lomnitz C (1970) Preliminary note: the Peru earthquake of may 31 1970. Bull Seismol Soc Am 60(4):1413–1416

Lomnitz C (1971) The Peru earthquake of may 31, 1970: some preliminary seismological results. Bull Seismol Soc Am 61(3):535–542

Mansinha L, Smylie E (1971) The displacement field of inclined faults. Bull Seismol Soc Am 61(5):1433–1440

Mas E, Adriano B, Pulido P, Jiménez C, Koshimura S (2014) Simulation of tsunami inundation in central Peru from future megathrust earthquake scenarios. J Disaster Res 9(6):961–967

Norabuena E, Leffler L, Mao A, Dixon T, Stein S, Sacks S, Ocola L, Ellis M (1998) Space geodetic observations of nazca-South America convergence across the central Andes. Science 279:358

Silgado E (1978) Historia de los sismos más notables ocurridos en el Perú (1513-1974). Instituto de Geología y Minería

Stauder W (1975) Subduction of the Nazca plate under Peru as evidenced by focal mechanisms and by seismicity. J Geophys Res 80(8):1053–1064

Villegas J, Chlieh M, Cavalie O, Baby P, Nouquet J (2016) Active tectonics of Peru: heterogeneous interseismic coupling along the Nazca megathrust, rigid motion of the peruvian sliver and subandean shortening accomodation. JGR 29:195–207